


Numerical investigation of rainfall-induced fines migration and its influences on slope stability

Xiaoqin Lei^{1,2,3}  · Zongji Yang¹ · Siming He^{1,3} · Enlong Liu² · Henry Wong⁴ · Xinpo Li¹

Received: 16 October 2016 / Accepted: 29 September 2017 / Published online: 17 October 2017
© Springer-Verlag GmbH Germany 2017

Abstract Rainfall-infiltration-induced fines migration within soil slopes may alter the local porosity and hydraulic properties of soils, and is known to be a possible cause of the failure of slopes. To investigate the intrinsic mechanisms, a mathematical formulation capable of capturing the main features of the coupled unsaturated seepage and fines migration process has been presented. Within the formulation, an unsaturated erodible soil is treated as a three-phase multi-species porous medium based on mixture theory; mass conservation equations with mass exchange terms together with the rate equations controlling fines erosion and deposition processes are formulated as the governing equations and are solved by the FEM method. The influences of both the fines detachment and deposition on the stability of slopes under rainfall infiltration have been investigated numerically. The results show that depending on whether the fines move out or get captured at pore constrictions, both desired and undesired consequences may arise out of the fines migration phenomenon.

It is suggested that more attention should be paid to those slopes susceptible to internal erosion whose safety analysis cannot be predicted by traditional methods.

Keywords Clogging · Fines migration · Rainfall infiltration · Slope stability · Suffusion · Unsaturated soil

1 Introduction

Soils in landslide deposits, colluvial slopes, and fill slopes sometimes show the geometrical features which are susceptible to seepage-induced internal erosion [2, 11, 21]. Under rainfall infiltration, fine particles in these broadly graded or gap-graded soils may be detached from the soil structure by the interstitial flow and transported with the flowing water within the pores formed by the coarse matrix [47]. The fines migration process will inevitably alter the local distribution of the size and content of fines in soils, lead to local variations of hydraulic and mechanical characteristics of soils within slopes [18, 29], and influence the instantaneous stability of slopes [38].

In the western mountainous area in China, this fines migration process during rainfall infiltration is known to be one of the main causes leading to the initiation of landslides and debris flows [12]. To investigate the mechanisms behind rainfall-induced failures in slopes comprised of these soils susceptible to internal erosion, both in situ artificial rainfall tests [3, 51] and laboratory flume tests [20, 46] have been performed. Generally, these tests at structure scale reported that, under rainfall infiltration, fines migrate from the upper and surface part of the slope towards the toe of slope; both surface coarsening and pore clogging phenomena can be observed due to fines

✉ Zongji Yang
yzj@imde.ac.cn

✉ Siming He
hsm@imde.ac.cn

¹ Key Laboratory of Mountain Hazards and Surface Process, Institute of Mountain Hazards and Environment, CAS, Chengdu 610041, China

² College of Water Resource and Hydropower, Sichuan University, Chengdu 610041, China

³ Center for Excellence in Tibetan Plateau Earth Sciences, CAS, Beijing 100101, China

⁴ Laboratoire de Génie Civil et Bâtiment, Ecole Nationale des Travaux Publics de l'Etat, Université de Lyon, 69120 Vaulx-en-Velin, France

migration; once fails, the slip surface is located at a very shallow depth above which the soils are nearly saturated, as shown in Fig. 1.

From a physical point of view, the fines migration in soils consists of the entire sequence of occurrences of release or detachment of fine particles, their motion with the flow, and finally their capture at some pore sites or their migration out of the medium under consideration [23]; simultaneously, the hydraulic and mechanical characteristics may also be altered, which make the fines migration in soils a complicated coupled multi-physics process. Extensive theoretical works have been performed to study the internal erosion properties of soils [14, 39, 44] and fines migration phenomena with applications in fields such as of Petroleum engineering and Hydraulic engineering [1, 5, 30, 32]. However, to date theoretical investigations of fines migration in related to slope stability are rare, especially the coupled analysis of rainfall infiltration into those unsaturated erodible soils. In view of this, Zhang and Zhang, [47] investigated the influences of internal erosion and particle transport on the unsaturated soil slope under rainfall infiltration with a coupled model of seepage and internal erosion based on the work of Cividini and Gioda [7]. The influence of fines migration on slope stability has been investigated by considering the effects of internal erosion on the change of porosity and saturated permeability. However, the possible pore clogging effects due to fines migration, which are considered as the main causes for the initiation of slope failures [12, 46], have not been considered in their work. Therefore, their model cannot explain the shallow failures demonstrated by some experimental works [3, 12, 46] (shown in Fig. 1).

In this paper, influences of both the fines detachment and deposition on the stability of slopes under rainfall infiltration have been investigated numerically. In the framework of continuum mixture theory, an unsaturated erodible soil is treated as a three-phase multi-species porous medium. Mass conservation equations with mass

exchange terms together with the corresponding rate equations for fines erosion and deposition are formulated as the governing equations and are solved by the FEM method. The classic Carman–Kozeny equation is modified to capture the permeability changes due to fines detachment and deposition. The numerical results show that depending on whether the fines move out or get captured at pore constrictions, two different sets of consequences occur. In the first case, the internal erosion leads to slope surface coarsening which promotes the dissipation of pore pressure, hence stabilizes the slope. In the second case, the deposition of in situ fluidized fines below the slope surface creates a relatively impermeable layer which leads to the generation of positive excess pore pressure and subsequent initiation the slope failure.

2 Mass conservation equations

2.1 Three-phase multi-species porous medium

Natural soils are usually unsaturated porous media, with a solid skeleton formed by their soil matrix and the pore spaces filled by liquid or air. As for the soils susceptible to suffusion, their soil matrix is usually composed of mixed coarse and fine particles. Under certain geometric and hydromechanical conditions [31], the fine particles can be detached from the solid skeleton and behave as a part of the liquid phase in the form of fluidized fine particles, which can be transported away by the flowing liquid. To describe these processes mathematically, an unsaturated erodible soil is treated as a three-phase multi-species porous medium. The tri-phasic porous medium contains solid phase S , liquid phase L , and gaseous phase G with their respective species, which can be summarised by the following sets.

$$S = \{c', e'\}; L = \{w, e\}; G = \{g\} \quad (1)$$

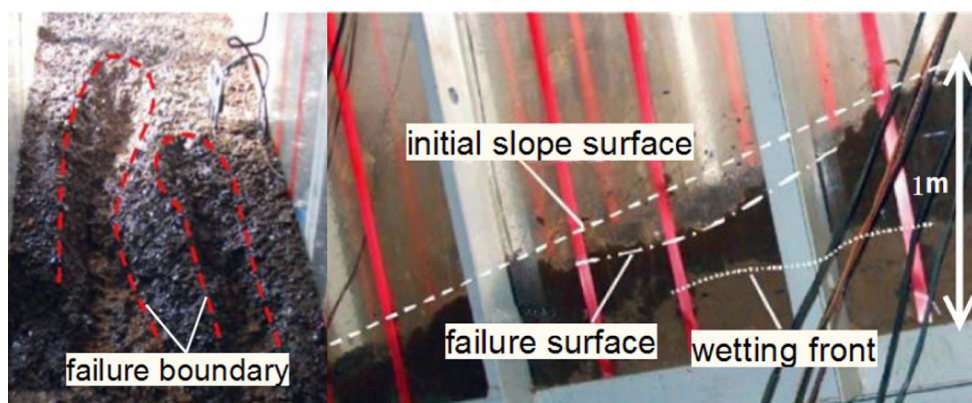


Fig. 1 Rainfall-induced failure of erodible slope in flume test [46]

in which “*c*’” is the coarse solid species, “*w*” is the water species, “*e*” is the fine species, and “*g*” is the air species. The superscript “’” indicates species that are attached to the solid phase, whereas no superscript is used to refer to species within the fluid phases. Due to erosion and deposition processes, the solid fine species *e*’ and fluidized fine species *e* can exchange mass with each other.

As shown in Fig. 2, at the initial instant *t* = 0, this tri-phasic porous medium, which occupies a volume *dΩ*₀ in the initial configuration, is taken as a reference representative volume. At an arbitrary time *t*, this soil element now changes to *dΩ*_{*t*} after the water infiltration. The Jacobian of the transformation of the solid phase *J* = *dΩ*_{*t*}/*dΩ*₀ is introduced to characterise this soil skeleton deformation. The total volume of the REV is the sum of individual volumes occupied by each species and can also be expressed as the sum of individual volumes occupied by each phase, such that, *dΩ*_{*t*} = ∑_{*j*} *dΩ*_{*t*}^{*j*} = ∑_{*α*} *dΩ*_{*t*}^{*α*} (“*j*”, “*α*” refer to a generic species and a particular phase, respectively). The Lagrangian volume fractions of a generic species *j* and of a particular phase *α* are defined as [24]:

$$\phi_j = d\Omega_t^j / d\Omega_0; \phi_\alpha = d\Omega_t^\alpha / d\Omega_0; \phi_\alpha = \sum_{j \in \alpha} \phi_j. \tag{2}$$

To be consistent with the terms used in the soil mechanics, the Lagrangian porosity *φ* is used to refer the Lagrangian volume fraction of the whole pore space; whereas the liquid saturation *S*_{*L*} is used to refer to the relative volume fraction occupied by the liquid within these pores; further, the volumetric concentration *c*_{*e*} is used to refer to the relative volume fraction of the fluidized fine particles in the liquid phase, such that:

$$\phi = \phi_L + \phi_G; S_L = \phi_L / \phi; c_e = \phi_e / \phi_L. \tag{3}$$

During water infiltration, both the saturation and porosity vary with time. At the time *t*, the volumes saturated by the liquid and gas phases have changed from their initial values to *S*_{*L*}*φdΩ*₀ and (1 - *S*_{*L*})*φdΩ*₀, respectively. Accordingly, the volume occupied by solid particles at time *t* can be calculated to be (*J* - *φ*)*dΩ*₀. By assuming that the net volume change due to the fines migration process is *φ*_{*e*}*dΩ*₀, from Fig. 2, the Lagrangian porosity *φ* at time *t* can be expressed as:

$$\phi = \phi_0 + (J - 1) + \phi_{er}. \tag{4}$$

This equation indicates that the variation of porosity is due to both the skeleton deformation and the fines migration. To further simplify the model, in the following paragraph, we will assume that the skeleton deformation during the water infiltration process is negligible (*J* - 1 ≈ 0). Hence, the porosity variations in this paper will be only due to the fines migration.

The macroscopic description necessitates the introduction of the concept of mass contents *m*_{*a*} as well as distinguishing apparent densities *ρ*^{*a*} from intrinsic densities *ρ*_{*a*} [49]. In all the following, *m*_{*a*}*dΩ*₀ = *ρ*^{*a*}*dΩ*_{*t*} denotes the actual mass of component “*a*” inside the current volume *dΩ*_{*t*}; hence, *m*_{*a*} = *Jρ*^{*a*}. Using the above notations, it can easily be deduced that:

$$m_S = (J - \phi)\rho_S; m_e = c_e S_r \phi \rho_e; m_w = (1 - c) S_L \phi \rho_w; m_G = (1 - S_L) \phi \rho_G. \tag{5}$$

In order to measure the relative variation of residual erodible fines *m*_{*e*}’ within the solid matrix, the mass fraction of fines *x*_{*e*}’ is introduced as:

$$x_{e'} = m_{e'} / m_{S0} \tag{6}$$

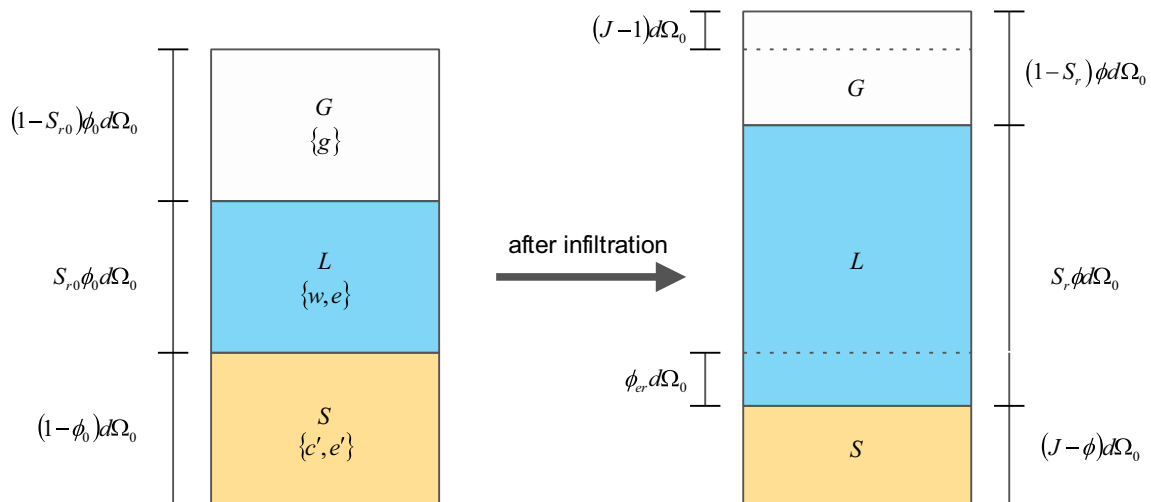


Fig. 2 Schematic illustration of initial and current volume fractions

in which the denominator is chosen as the initial mass content of solid phase m_{s0} rather than its current counterpart which varies along with the fines migration.

2.2 Conservation equations for liquid and fine species

By privileging the solid phase, the general continuity equation of a generic species j under infinitesimal transformation can be given as [24, 26]:

$$\frac{d^s}{dt} m_j + \nabla \cdot \mathbf{J}^j = \hat{m}_j \quad (7)$$

in which $\frac{d^s}{dt}$ is the particle derivative with respect to the solid phase [10]; \hat{m}_j is the mass growth rate of species j per unit initial overall volume $d\Omega_0$; \mathbf{J}^j is the volume flux of species j relative to the solid skeleton. The above equation indicates that the mass change of a species j occupying the same spatial region as a given solid skeleton is indeed due to two physical phenomena: the creation of species due to physical–chemical reactions (the erosion and deposition of fines in our case) and the net influx of the species due to their relative velocity [26]. To simplify the model, all the species are assumed intrinsically incompressible ($\rho_j = cst$) [24]; it can be reformed as:

$$\frac{d^s}{dt} \phi_j + \nabla \cdot \mathbf{J}^j = \frac{\hat{m}_j}{\rho_j} \quad (8)$$

Since only fluidized fine particles can exchange mass with their counterparts in the solid phase, with the relation $\mathbf{J}^L = \sum_{j \in L} \mathbf{J}^j$ for the volume flux of liquid phase L [24] and Eq. (2) $\phi_L = \sum_{j \in L} \phi_j$, the continuity equation for liquid phase L can be presented as:

$$\frac{d^s}{dt} \phi_L + \nabla \cdot \mathbf{J}^L = \frac{\hat{m}_e}{\rho_e} \quad (9)$$

Under the assumption that the same type of species shares the same density in both solid phase and liquid phase ($\rho_e = \rho_{e'}$), the RHS term in the above equation \hat{m}_e/ρ_e is equal to the net porosity change rate $\dot{\phi}_{er}$ due to the fines migration (note that $\hat{m}_e = -\hat{m}_{e'}$). Then, the substitution of the above equation into the differential of $\phi_L = S_L \phi$ leads to:

$$\frac{(1 - S_L)}{\rho_{e'}} \frac{d^s}{dt} m_{e'} + \phi \frac{d^s}{dt} S_L + \nabla \cdot \mathbf{J}^L = 0. \quad (10)$$

In this work, the air pressure is assumed to remain at atmospheric pressure by simply setting $p_G = 0$. Hence, the matric suction $p_c = -p_L$. By assuming that the saturation S_L depends only on matric suction p_c , S_L is a function which relies only on the liquid pressure p_L .

$$\frac{(1 - S_L)}{\rho_{e'}} \frac{\partial}{\partial t} m_{e'} + \phi \frac{\partial S_L}{\partial p_L} \frac{\partial p_L}{\partial t} + \nabla \cdot \mathbf{J}^L = 0. \quad (11)$$

The substitution of $\phi_e = c_e S_L \phi$ into Eq. (8) and further the use of the continuity Eq. (9) lead to:

$$\nabla \cdot \mathbf{J}^e - c_e \nabla \cdot \mathbf{J}^L + \frac{1 - c_e}{\rho_{e'}} \frac{\partial}{\partial t} m_{e'} + S_L \phi \frac{\partial}{\partial t} c_e = 0. \quad (12)$$

The fluidized fines can be transported by both the advection and diffusion mechanisms. In our case, it is assumed that the fines transport due to the diffuse mechanism is negligible. Hence, the relation $\mathbf{J}^e = c_e \mathbf{J}^L$ holds [24]. The substitution of it into the above equation leads to:

$$\frac{1 - c_e}{\rho_{e'}} \frac{\partial}{\partial t} m_{e'} + S_L \phi \frac{\partial}{\partial t} c_e + \mathbf{J}^L \cdot \nabla c_e = 0. \quad (13)$$

3 Rate equations for erosion and deposition

3.1 Mechanisms of erosion and deposition

The fines migration process in soils is a particle-scale phenomenon, which concerns the detachment, transport, and deposition of individual fine particles. For the illustration purpose, the soils considered here can be roughly approximated as a network of pore chambers, i.e. pore bodies connected through pore throats (i.e. pore constrictions) [28]. As illustrated in Fig. 3, during the flow of a permeating liquid through these soils, fine particles attached to pore surfaces are released or detached under certain sets of conditions by colloidal or hydrodynamic forces [5]. Once the fines are released, the particles move with the permeating liquid until they get retained at other locations (pore throats, regular pore surfaces, etc.) in the soil skeleton or exit the soil skeleton [23].

Fine particles can be captured by either the pore surface deposition or pore throat blocking [25]. Pore surface deposition refers to the relatively uniform deposition of particles, whose sizes are much smaller than pore sizes, on pore surfaces due to various forces. Pore throat blocking occurs stochastically when a single particle plugs or several particles bridge at pore throats [5]. The release of fines from one place of pore bodies and subsequent deposition at another place of pore bodies usually cannot alter the permeability of the porous medium significantly, but severe permeability damage can result from the entrapment of fines at pore throats [25]. Plugging of pore throats by blocking and bridging may cause some pore throats to close for flow. What's more, once the convective pore throat blocking occurs, particles may begin accumulating behind the pore jamming particles by a snowball effect (i.e. filter cake formation) [16]. The main concern of this paper

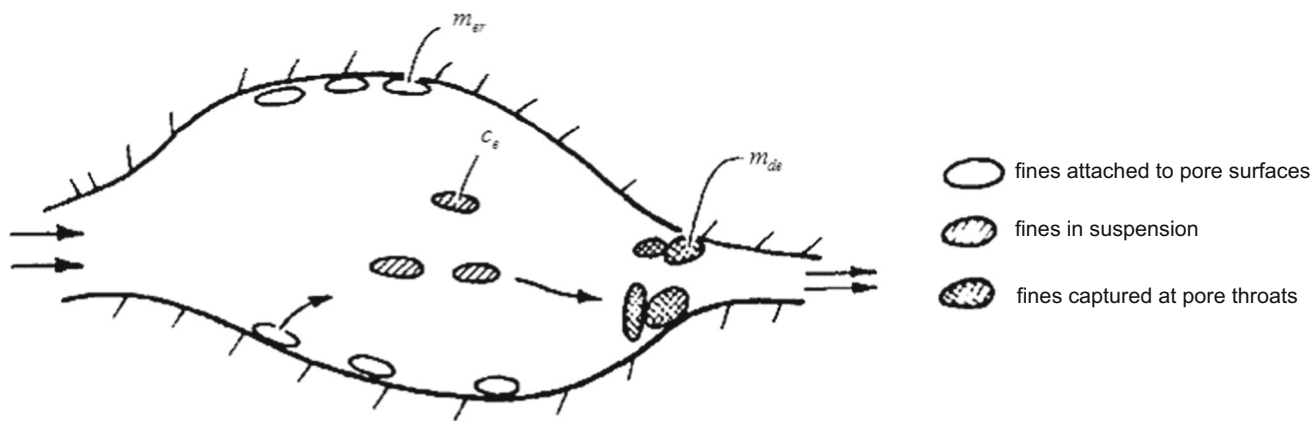


Fig. 3 Schematic diagrams of pore-fine system during water flow [22]

is to investigate the variation of permeability distribution profiles in soil slopes during the rainfall-induced fines migration process. Since pore throat plugging causes more severe permeability impairment than pore surface deposition [5], consistent with Liu and Civan, [25], in the following it is assumed that pore surfaces (mainly pore bodies) are the sites for the mobilisation of in situ fines and pore throats are the sites for the capture of mobilised fines. Consequently, the variation of fines content is assumed to be due to the detachment of fines available at pore surfaces and the plugging and subsequent pore filling at pore throats.

$$\dot{m}_{e'} = \dot{m}_{er} + \dot{m}_{de} \tag{14}$$

In view of this equation, the variation of fines mass content $\dot{m}_{e'}$ in Eqs. (11) and (13) is assumed due to these two processes accordingly, whose rate equations (\dot{m}_{er} and \dot{m}_{de}) should be given separately. Based on experimental studies, numerous phenomenological rate equations governing these processes have been proposed and are reviewed for the applications in many different fields [6, 8, 29, 34]. In the absence of specified experimental results, the rate equations used in this paper are directly taken from the literature and are presented below.

3.2 Erosion law

For the sake of simplicity, the detachment considered here is only due to the hydrodynamic mechanism. At the pore scale, the fines detachment is related to the shear stress exerted by the flowing pore fluid, the erosion resistance of the specified soils, and the amount of available erodible fine particles on the pore surfaces. Similar to Uzuoka et al. [42] and Zhang & Zhang [47], the erosion law proposed by Cividini and Gioda [7] has been modified to govern the fines detachment in both saturated and unsaturated soils.

$$\frac{\partial m_{er}}{\partial t \rho_{e'}} = -k_e \cdot (x_{e'} - x_{e'\infty}) \cdot \|\mathbf{v}^{wS}\| \tag{15}$$

in which k_e is a positive material constant reflecting the sensitivity of the soil to hydrodynamic forces; $\|\mathbf{v}^{wS}\|$ is the norm of the relative velocity vector of pore water to soil skeleton; $x_{e'}$ is the current mass fraction of erodible fines defined by Eq. (6); $x_{e'\infty}$ is the ultimate mass fraction of erodible fine particles which is a decrease function of liquid flow velocity [42] and is approximated as [7]:

$$\begin{aligned} x_{e'\infty} &= x_{e'0} - (x_{e'0} - x_{e'\infty}^*) \frac{\mathbf{v}^{wS}}{\mathbf{v}^*} & \text{if } 0 \leq \mathbf{v}^{wS} \leq \mathbf{v}^* \\ x_{e'\infty} &= x_{e'\infty}^* - \alpha_{er} \cdot \log\left(\frac{\mathbf{v}^{wS}}{\mathbf{v}^*}\right) & \text{if } \mathbf{v}^{wS} > \mathbf{v}^* \end{aligned} \tag{16}$$

where \mathbf{v}^* is a reference constant velocity of pore water, under which the erosion process is very slow; $x_{e'\infty}^*$ is the ultimate mass fraction of fine particles under this velocity; $x_{e'0}$ is the initial mass fraction of fine particles before erosion; α_{er} is a parameter of erosion, which controls the decreasing rate of $x_{e'\infty}$ with increasing flow velocity \mathbf{v}^{wS} .

3.3 Deposition law

The detached fines flow with the invading liquid as suspension and may deposit either at the pore surfaces or pore throats subsequently. Gruesbeck and Collins [16] have reported that for surface deposition, there exists a critical velocity, below which only particle retention takes place and above which retention and entrainment of fine particles occur simultaneously. The fines which deposit at the pore surfaces influence the hydromechanical properties of soils slightly by narrowing the flow pathways. Hence, the surface deposition process is assumed to be partially accounted for by adjusting the surface erosion process and will not be considered explicitly here. The rate of the capture of fluidized fines at pore throats is assumed

proportional to the particle flux [25], i.e. the probability of infiltration increases with an increasing number of particles, which pass through the REV per time unit [37], which is given by:

$$\frac{\partial m_{de}}{\partial t \rho_e} = k_d \cdot c_e \cdot \|\mathbf{v}^{wS}\| \quad (17)$$

in which k_d is a measure of the retention capacity of the fluidized fines at pore throats; c_e is the volumetric concentration of fluidized fines in the suspension; $\|\mathbf{v}^{wS}\|$ is the norm of the relative velocity vector of pore water, which is also presented in Eq. (15).

4 Governing equation for liquid flow

4.1 Darcy's law

For the internal erosion problem considered here, the fines are mainly detached by hydrodynamic forces and transported by the advection of the permeating water. Though diffusion of smaller fines may take place within the water, its contribution to the total fines migration process is relatively negligible compared with the advection mechanism and has been neglected. The classic Darcy's law is presented here to calculate the volume fluxes of the liquid phase \mathbf{J}^L [24, 42]:

$$\mathbf{J}^L = -\frac{K_h}{\gamma_L} (\nabla p_L - \gamma_L) \quad (18)$$

in which γ_L is the specific weight of pore water, which is assumed to be constant here for simplicity; K_h is the hydraulic conductivity, which has been recognised as one of the key parameters in the seepage and slope stability analysis involving unsaturated soils [33, 41]. It is assumed to be expressed as:

$$K_h = K_{h0} K_{rl}(S_L) K_{rl}(\phi, m_{de}, c_e) \quad (19)$$

in which K_{h0} is the initial hydraulic conductivity; $K_{rl}(S_L)$ and $K_{rl}(\phi, m_{de})$ are dimensionless coefficients which phenomenologically reflect the effects of liquid saturation and erosion on the hydraulic conductivity.

4.2 Effects of saturation

When water infiltrates into unsaturated soils, parts of water will be retained by capillary forces. The specific water capacity is calculated from the soil water characteristic curve (SWCC), which is assumed to be fitted by the Van Genuchten's equation [43]:

$$S_L = S_{\min} + (S_{\max} - S_{\min}) [1 + (\alpha_v p_c)^{n_v}]^{-1/n_v} \quad (20)$$

in which S_L is the liquid saturation; p_c is the matric suction; S_{\min} and S_{\max} are the minimum (residual) and maximum saturation can be reached; α_v and n_v are fitting parameters.

The unsaturated coefficient $K_{rl}(S_L)$ is introduced to reduce the hydraulic conductivity and accounts for the combined effects due to tortuosity and drag forces in unsaturated soils and takes a value between 0 and 1 [15].

$$K_{rl}(S_L) = \exp(-\alpha_v p_c). \quad (21)$$

4.3 Effects of fines migration

The Carman–Kozeny equation is widely used to relate the intrinsic permeability to the changes of porosity. However, it was found experimentally that this equation fails to represent the cases where the pore throats are plugged without significant porosity reduction [5]. Indeed, the detachment of fines yields insignificant increase in permeability, while clogging of fines at pore throats causes significant reduction in permeability [5]. Meanwhile, the increasing fines concentration in fluid may also change the soil conductivity by increasing the fluid viscosity [13, 49]. By modifying the original Kozeny–Carman equation and taking into account the above-mentioned effects, based on the works of Liu and Civan [25], Fujisawa et al., [13] and Sbai and Azaroual [36], the following expression for the instantaneous permeability change by the release and retention of particles is adopted:

$$K_{rl}(\phi, m_{de}, c_e) = \frac{[(1 - f_r)K_f + f_r \phi / \phi_0]^{n_r}}{1 + 2.5c_e} \quad (22)$$

in which K_f is a parameter accounting for the residual permeability of the plugged formation enabling therefore the so-called gate or valve effect of the pore throats; n_r is an index which is claimed to be in the range between 2.5 and 3.5; f_r is a flow efficiency factor, which is defined as the fraction of the unplugged available for liquid flow, and is expressed empirically as a linear function of the mass of particles captured at pore throats [25]:

$$f_r = 1 - k_r m_{de} \quad (23)$$

where k_r is the coefficient of flow efficiency for fine particles.

5 Numerical analysis of effects of fines migration on the slope stability

Under rainfall infiltration, shallow failures of slopes may be triggered due to the decrease in matrix suction along with the advancement of a wetting front in the unsaturated soils [48]. If the soils comprising the slopes are composed of mixed coarse and fine particles which exhibit a

geometrical characteristic prone to internal erosion [2], fine particles may be detached and transported with the permeating water inside the slopes under heavy rainfall infiltration [11, 47]. The migration of fines out of their initial soil skeletons changes the porosity and permeability of soils, and may further affect the water infiltration process and hence the stability state of slopes. Intuitively, the stability analysis of slopes subjecting to fines migration should be different from that of slopes without internal erosion. To investigate the influences of fines migration on the stability of unsaturated slopes under rainfall infiltration, in the following, the rainfall infiltration processes in unsaturated erodible soils are simulated with the formulation presented; the effects of fines erosion and deposition on the infiltration processes and the slope stability are investigated carefully.

5.1 Governing equations and infinite slope model

Four governing equations presented previously are summed up and implemented into the FEM code BIL, developed by Prof. P. Dangla (<http://perso.lcpc.fr/dangla.patrick/bil/>) for the simulations, which include the mass conservation equation of liquid phase, the mass conservation equation of fluidized fines, the erosion rate equation, and the deposition rate equation. The four main unknowns are selected as the liquid pore pressure p_L , the volumetric concentration of fluidized fines c_e , the mass content of fines at pore surface m_{er} , and the mass content of fines at pore throats m_{de} .

$$\begin{aligned} \frac{(1 - S_L)}{\rho_{e'}} \frac{\partial}{\partial t} (m_{er} + m_{de}) + \phi \frac{\partial S_L}{\partial p_L} \frac{\partial p_L}{\partial t} + \nabla \cdot \mathbf{J}^L &= 0, \\ S_L \phi \frac{\partial}{\partial t} c_e + \frac{1 - c_e}{\rho_{e'}} \frac{\partial}{\partial t} (m_{er} + m_{de}) + \mathbf{J}^L \cdot \nabla c_e &= 0, \\ \frac{\partial m_{er}}{\partial t} \frac{1}{\rho_{e'}} &= -k_e \cdot (x_{e'} - x_{e'\infty}) \cdot \|\mathbf{v}^{wS}\|, \\ \frac{\partial m_{de}}{\partial t} \frac{1}{\rho_{e'}} &= k_d \cdot c_e \cdot \|\mathbf{v}^{wS}\|. \end{aligned} \quad (24)$$

Since slope failures induced by rainfall infiltration are usually shallow, the slope stability can be evaluated by the infinite slope model shown in Fig. 4, with the assumption that the groundwater table depth is kept constant during the rainfall infiltration process [47, 48]. The infiltration process is assumed to modify the stability state of slopes by changing the pore water pressure profiles [48]. A factor of safety F_s under steady vertical seepage for both saturated and unsaturated conditions with the inclusion of the suction stress is given by Lu and Godt [27]:

$$F_s = \frac{\tan \varphi}{\tan \beta} + \frac{2c}{\gamma H_{ss} \sin 2\beta} - \frac{\sigma_s}{\gamma H_{ss}} (\tan \beta + \cot \beta) \tan \varphi \quad (25)$$

in which c is the effective cohesion; φ is the effective friction angle; β is the slope angle; H_{ss} is the vertical depth at the failure surface; γ is the unit weight of soil; σ_s is the suction stress defined by:

$$\sigma_s = -\frac{S_L - S_{\min}}{1 - S_{\min}} P_c = \frac{S_L - S_{\min}}{1 - S_{\min}} P_L. \quad (26)$$

For the sake of simplicity, it is assumed that the cohesion and friction angle are independent of matric suction and fines content, and the depth-averaged unit weight of soil can be represented by a constant averaged value (which are the assumptions adopted by the majorities [40]). Therefore, the variation of safety factor is totally due to the change of the so-called “suction stress” σ_s .

Within the unsaturated zones, the vertical rainfall infiltration dominates [19]; hence, only downward fines migration process is under consideration. By assuming that each slice of an infinitely long slope is subjected to the same amount and intensity of rainfall, an individual slice can be then treated as a one-dimensional soil column subject to vertical infiltration [9]. In view of this, the slope stability can be evaluated by Eq. (25) with the coupled term—the so-called “suction stress” σ_s updated in time and space during the rainfall infiltration process.

5.2 Material parameters

The soil under investigation in this work is based on the surface layers of slopes at the debris flow source area of Jiangjia Ravine, which is a kind of unsaturated weak-cohesion broadly graded gravelly soils. The initial porosity and dry density of the soil are about 0.36 and 1700 kg/m³, respectively. The clay (< 0.005 mm) and silt (0.005–0.075 mm) particles account for 6.78 and 13.35% by weight (as shown in Fig. 5), and its main clay mineral composition of fine fraction is chlorite and illite [45]. The uniformity coefficients C_u of this soil is much > 20 and is considered as internally unstable [45]. As reported by Chen [3] and Wang et al. [46], fines migration process will take place within these soils under rainfall infiltration.

The parameters regarding to the fines erosion and deposition as well as their induced permeability changes are calibrated by a set of constant-head permeability tests performed by Wang [45]. The size of specimens in the tests is 20 cm height and 19 cm diameter. Five piezometer tubes were installed, which divided the specimens into four equal-length sections. The permeability evolution of each section during the tests can therefore be monitored. As shown in Fig. 6, by imposing 5-cm constant water head on the top surface of the

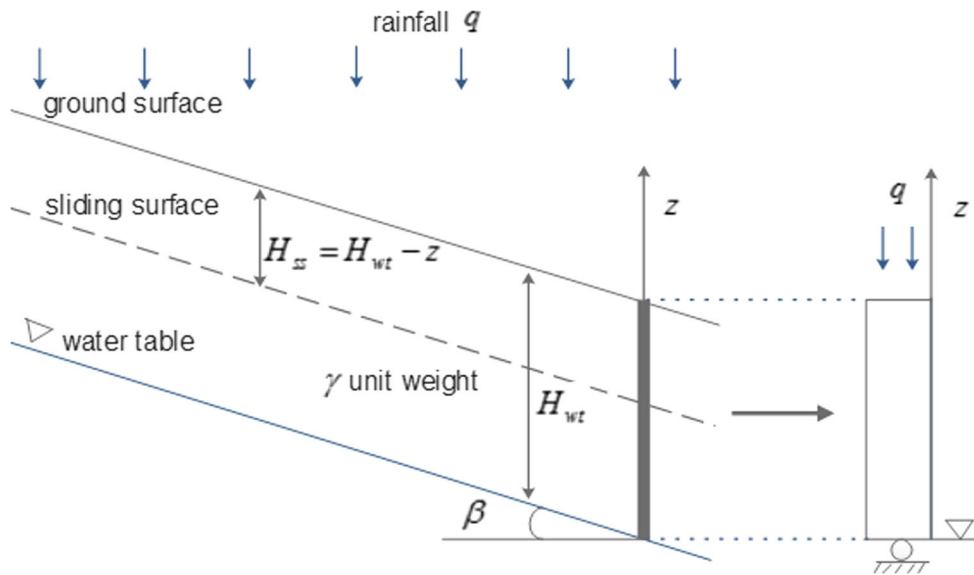


Fig. 4 Infinite slope model

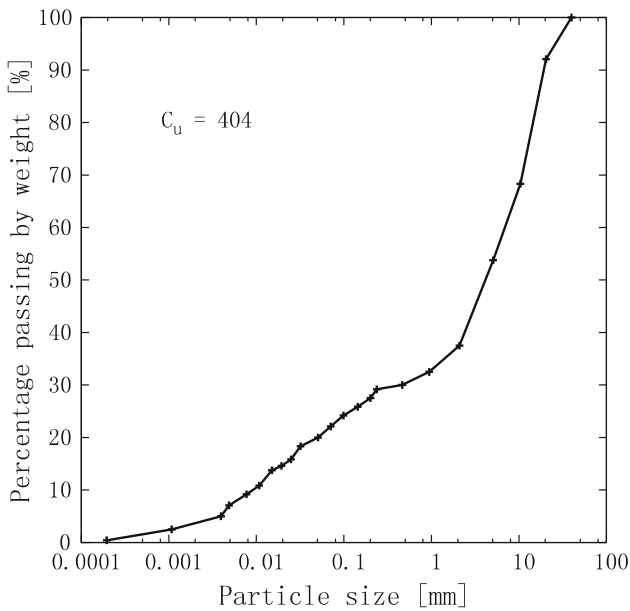


Fig. 5 Grain-size distribution of Jiangjia Ravine soil [45]

specimen, with the bottom surface maintaining at air pressure, both the induced water flux and the permeability ratio (current permeability/original permeability) of each section evolve with time. During the test, the permeability of the top and mid-upper sections increased gradually with time, which were opposite for the bottom and mid-lower sections; the global permeability of the specimen increased slightly, especially at initial times. It is concluded by Wang [45] that such kind of permeability evolution is due to the coupled suffusion and clogging process within the sample. As also shown in Fig. 6, by adopting the parameters in Table 1, the model proposed in this paper can reproduce the flux and permeability ratio

evolution curves quite satisfactorily. The parameters for Van Genuchten’s equation are obtained by best fitting of the SWCC curves for classic deposited soils presented in Zhou et al. [50] which have similar porosity and compositions with the soils studied. The cohesion and friction angle of the soil as well as the slope angle are also selected with reference to the ones presented in Wang [45] (Table 2).

5.3 Infiltration in unsaturated columns

Here, a 6-m unsaturated soil column ($H_{wt} = 6$ m) is under consideration. The initial and boundary conditions are presented by Eq. (27). The initial pore water pressure distribution is considered to be linear. The water level is assumed to be located at the bottom of the soil column where the boundary conditions for water are permeable and the pore water pressure is equal to zero. The initial mass contents of fine particles deposited at the pore surfaces and pore throats are assumed to be 340 kg/m^3 and 0, respectively. No fluidized fines exist in the pore water before infiltration ($c_e = 0$). At time $t = 0^+$, a rainfall (clean water) flux with the intensity 90 mm/h is suddenly applied at the top boundary. This hydraulic loading will induce penetration of water into the unsaturated soil column via the top boundary and subsequent fines migration process.

$$\begin{aligned}
 p_L(z, t = 0) &= -\gamma_L z \text{ kPa}; m_{er}(z, t = 0) \\
 &= 340 \text{ kg/m}^3; m_{de}(z, t = 0) = 0 \text{ kg/m}^3; \\
 c_e(z, t = 0) &= 0; \mathbf{J}^L(z = 6 \text{ m}, t > 0) \\
 &= -90 \text{ mm/h}; c_e(z = 0, t > 0) = 0.
 \end{aligned}
 \tag{27}$$

For the illustration purposes, three cases are simulated: (1) infiltration without fines migration ($k_e = k_d = 0$); (2)

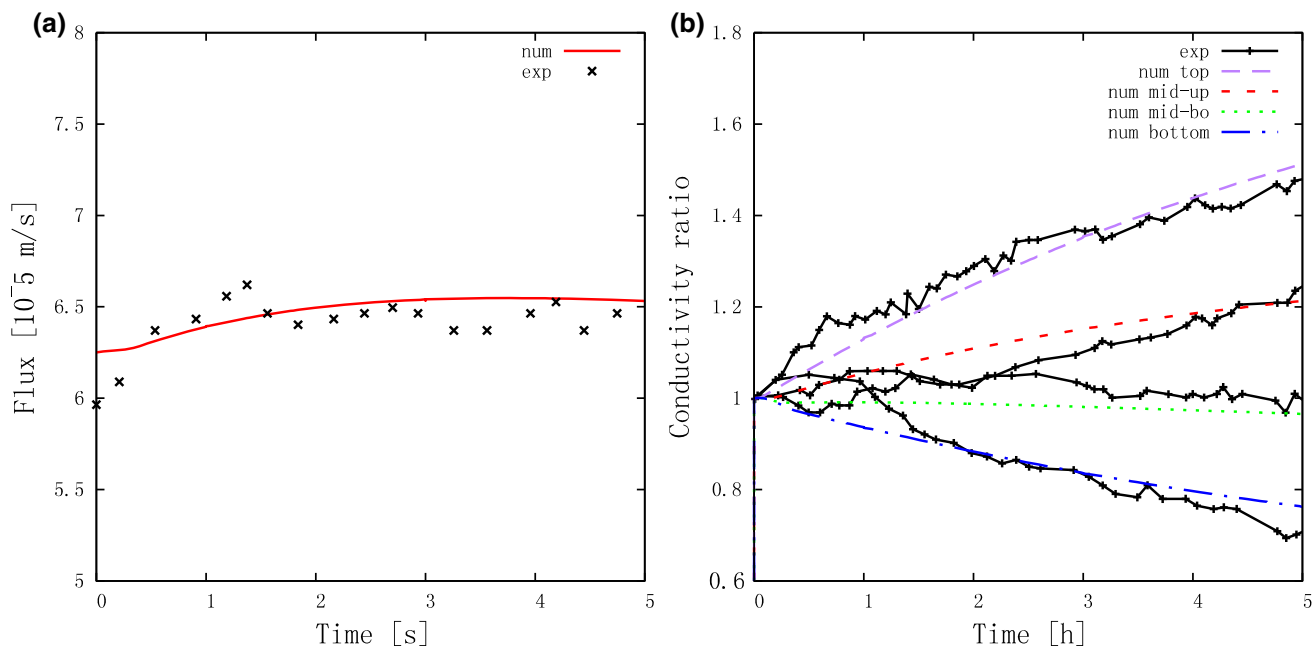


Fig. 6 Evolution of flux and permeability ratio during the permeability test. **a** Evolution of flux; **b** evolution of permeability ratio

Table 1 Parameters for the coupled model

K_{h0} (m/s)	γ_L (kN/m ³)	ϕ_0	n_r	K_f	k_r	$m_{e'0}$ (kg/m ³)	S_{min}	S_{max}
5. e-5	10	0.36	3	0	0.05	340	0	0.97
k_e	$x_{e'0}$	$x_{e'\infty}^*$	v^* [m/s]	α_{er}	k_d	$\rho_{e'}$ [kg/m ³]	α_v	n_v
0.4	0.2	0.19	5.e-6	0.1	0.2	2600	0.05	1.8

Table 2 Parameters for infinite slope

c (kPa)	φ (°)	β (°)	γ (KN/m ³)
6	25	25	24

infiltration with pure erosion ($k_e = 0$); and (3) infiltration with simultaneous erosion and deposition of fines. The numerical results of case 2 and case 3 with comparison to those of case 1 are presented in the following paragraph.

(1) Effects of fines erosion (case 2 vs. case 1)

Along with the advancement of the wetting front, the erodible fines at pore surfaces are detached and transferred to the fluidized fines, which are entrained by the flowing water downward by advection. The infiltrating rate in the unsaturated soil column increases along with the wetting process which leads to the inhomogeneous erosion profiles as shown in Fig. 7a, other than that of the saturated case [42]. When the wetting front goes deeper, more fines are entrained along the flow path, which is indicated by the increasing peak concentrations shown in Fig. 7b.

With the absence of mechanical deformation, the porosity variation is purely induced by the variation of fines content [according to Eq. (4)]. As shown in Fig. 8a, the porosity increases with the fines detachment (erosion) process simultaneously. In this example, it is assumed that once the fine particles are detached from the pore surfaces, they will be transported downwards without any possible deposition (pore throat blockage and filling are neglected). Therefore, the permeability is controlled by the variations of porosity, liquid saturation, as well as liquid viscosity. As shown in Fig. 8b, the permeability ratio variation profiles with erosion (coloured curves) and without erosion (grey curves) are plotted in one figure for the comparison purpose. The permeability variation without erosion is solely due to the wetting process by changing the liquid saturation. As can be seen from the grey curves, the wetting process increases the liquid saturation which gives more space for water transportation at constant porosity, which further increases the permeability. Beside the saturation process, the erosion process will increase the porosity, which leads to more significant permeability increase in the

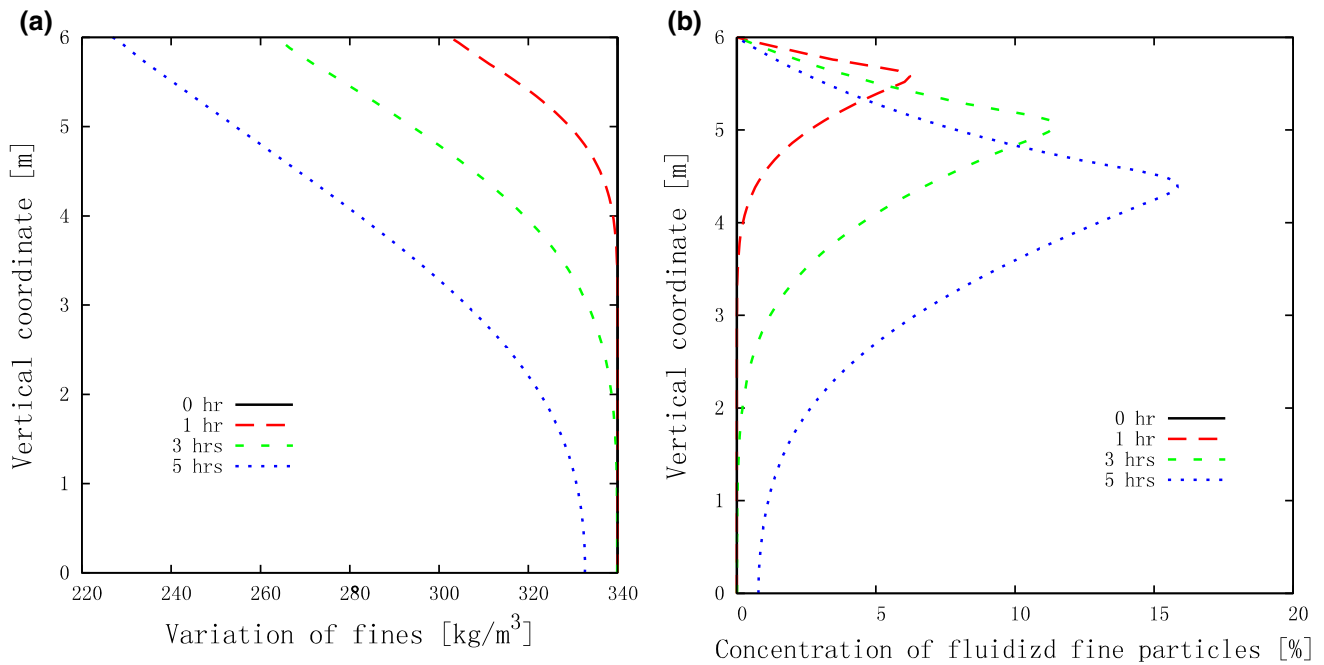


Fig. 7 Profiles of mass content of erodible fines and concentration of fluidized fines in case 2. **a** Mass content of erodible fines; **b** volumetric concentration of fluidized fines

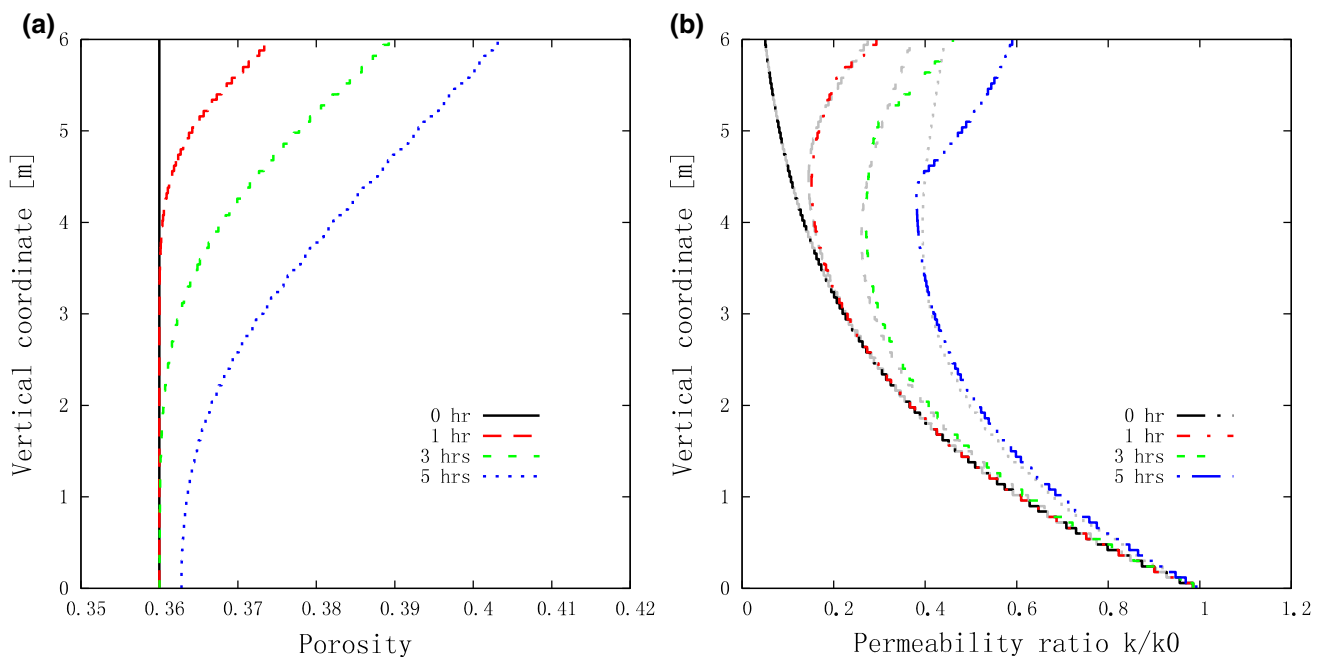


Fig. 8 Profiles of porosity and permeability ratio in case 2. **a** Evolution of porosity; **b** evolution of permeability ratio

upper regions with severe erosion (i.e. “surface soil coarsening” as reported by Cui et al. [12]).

The increase in permeability due to erosion facilitates the water infiltration, as shown in Fig. 9a. At larger times, the liquid volume increased by rainfall flux is less than the pore volume created by severe erosion near the top surface, which leads to an evident decrease in saturation in the top

regions. The pore pressure profiles are related to the saturation profiles bijectively by the soil–water characteristic curve (Eq. 20). Accordingly, as shown in Fig. 9b, compared with the ones without erosion (grey curves), the negative pore pressures dissipate more rapidly due to the erosion-induced permeability increase. What’s more, after

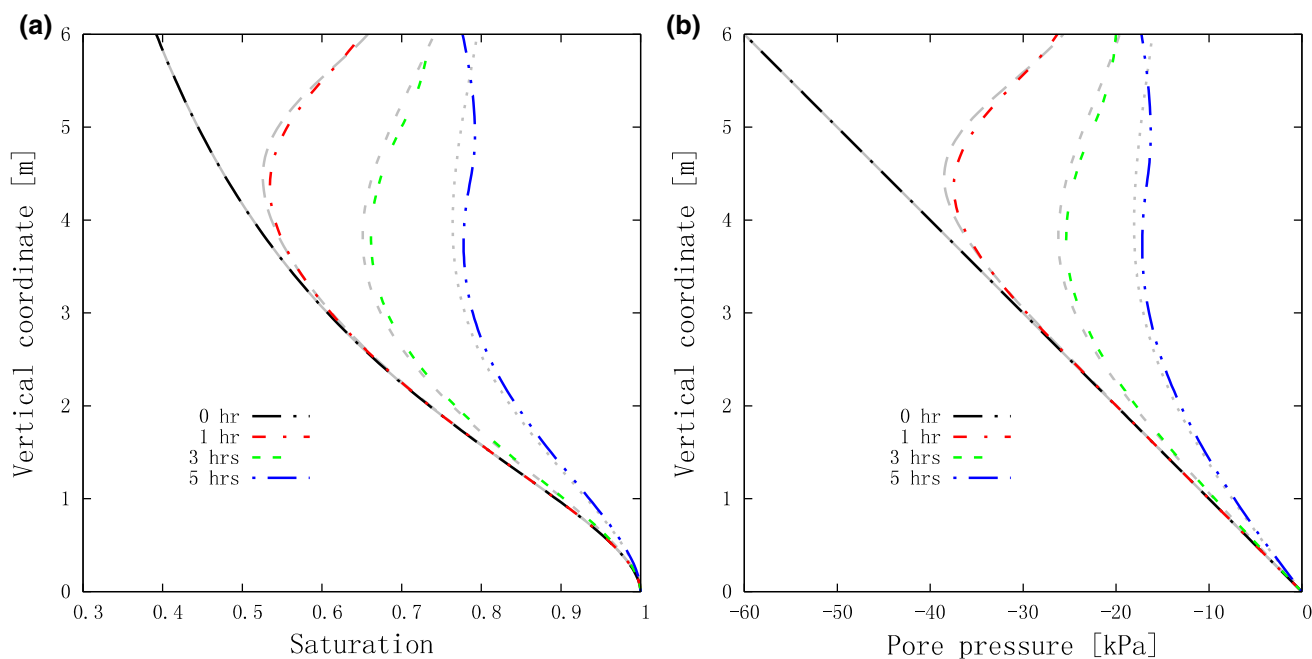


Fig. 9 Profiles of liquid saturation and pore pressure in case 2. **a** Saturation; **b** pore pressure

erosion the coarsened top regions with lower saturations show larger capillary pressures.

(2) Effects of fines erosion and subsequent deposition (case 3 vs. case 1)

In a more realistic situation, the fine particles entrained by the flowing liquid in the upper region will be partly recaptured and deposited in the deeper region. This numerical example presented here is intended to illustrate the combined effects of fine detachment and subsequent deposition. Similar to the previous case without deposition, when the clear water infiltrates into the soil column, the erodible fines are detached (Fig. 10a) and transferred into the fluidized fines, which are entrained by the flowing water downward by advection (Fig. 10b). The comparison of Fig. 10 with Fig. 7 shows that the difference of erosion intensity (which is mainly controlled by the infiltration rate at pore scale) between two cases is small. However, the difference of concentration of fluidized fines between these two cases is significant: the peak concentrations in case 3 are nearly half of those in case 2.

When the deposition process is taken into account, parts of fluidized fine particles will be caught by the pore throat blocking and filling mechanisms at the pore throats and transferred into solid deposition (as shown in Fig. 11a). According to Eq. (17), the deposition rate is proportional to the fluidized fine particle flux. Once the fines concentration increases, the chance of pore throat interception increases simultaneously. Since clean water is injected into the soil column, the fines concentration at the top surface is always

zero, so as the deposition rate. Deeper inside the soil column, along with the advancement of fines suspension, the content of fines deposition increases correspondingly with time. Always, a peak value of deposition content exists at the shallow depth near the top surface. This is a reasonable result according to our model: above of this region, fines concentration is relatively lower due to the mixture of clean water from the top surface, which leads to a lower deposition rate; below this region, the wetting front of particle flux reaches later; hence, the deposition time is shorter.

The distribution profiles of the total fines remained in the soil matrix are obtained by a simple addition of the profiles of the residual erodible fines (Fig. 10a) and those of the fines deposition (Fig. 11a), which are plotted in Fig. 11b. Overall, the soil columns have lost fine particles everywhere, especially in the upper regions. According to Eq. (4), the porosity profiles can be obtained from Fig. 11b which are shown in Fig. 12a. In the upper region which is subjected to less deposition, the porosity increases significantly and is compatible with Fig. 8a in magnitude. However, in the deeper regions the porosity increase in this case (case 3) is less than that of the case without deposition (case 2). This is due partially to the fact that the deposition process compensates partially the erosion effect and also due partially to the permeability impairment which decreases significantly the flow flux in the deeper regions (hence lower erosion rate).

As shown in Fig. 12b, the permeability ratio evolution profiles in this case (coloured curves) together with the

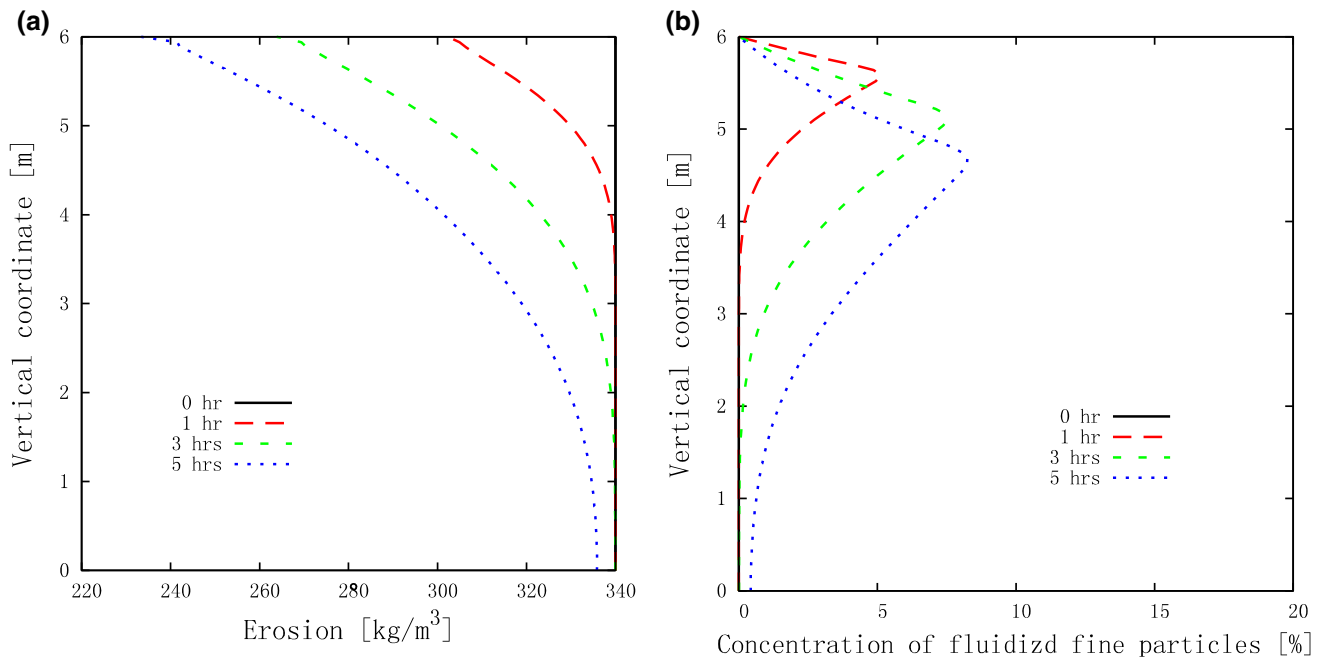


Fig. 10 Profiles of mass content erodible fines and concentration of fluidized fines in case 3. **a** Mass content of erodible fines; **b** volumetric concentration of fluidized fines

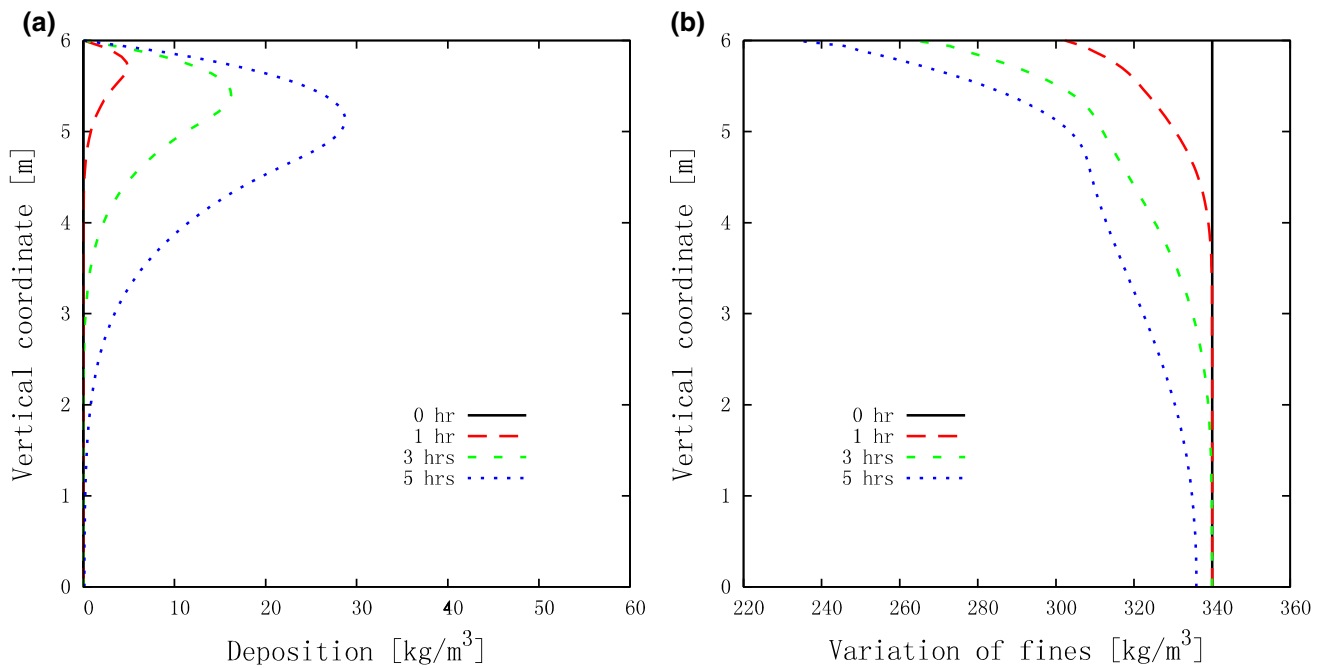


Fig. 11 Profiles of deposited and total fine content in case 3. **a** Mass content of fines deposition; **b** mass content of total fines

ones without fines migration (grey curves) are presented. According to the modified Kozeny–Carman equation (Eq. 22): on the one hand, the overall increase in porosity tends to increase the permeability; on the other hand, the fines deposited due to the throat blockage and pore filling at pore throats tend to decrease the permeability. The two mechanisms compete with each other within the whole soil

column. As can be seen in Fig. 12b, in the upper region (about 0–0.5 m in depth) where the porosity increases significantly and the deposition rate is small, the permeability in this case increases more significantly than the ones without fines migration, which will facilitate the water infiltration. A little deeper in the region where the fines deposition concentrates (as shown in Fig. 11a), the

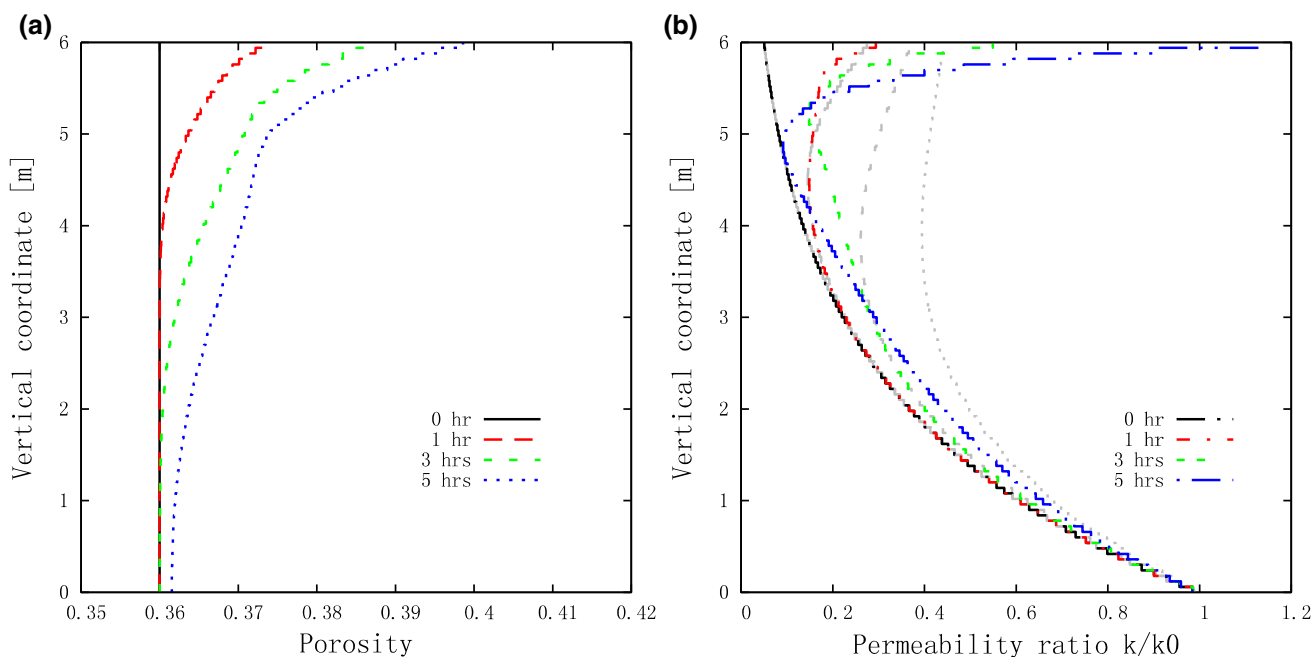


Fig. 12 Profiles of porosity and permeability ratio in case 3. **a** Evolution of porosity; **b** evolution of permeability ratio

permeability in this case decreases more significantly compared with the ones without fines migration, which will prevent the downward water infiltration.

Under constant infiltration rate, the saturation profiles (wetting front advancement) are significantly influenced by the permeability evolution. As shown in Fig. 13a, compared with the case without fines migration (grey curves), the wetting process is significantly retarded when the

deposition region grows denser at large times. Within this region, water infiltrates downwards with a much lower rate than the inputting water flux rate from the upper regions which have been enhanced by the erosion-induced porosity increase. As a result, water starts to accumulate above this dense deposition region at larger times. As clearly shown in this figure, under a rainfall flux smaller than the soil saturated permeability, after < 5 h, the upper regions have

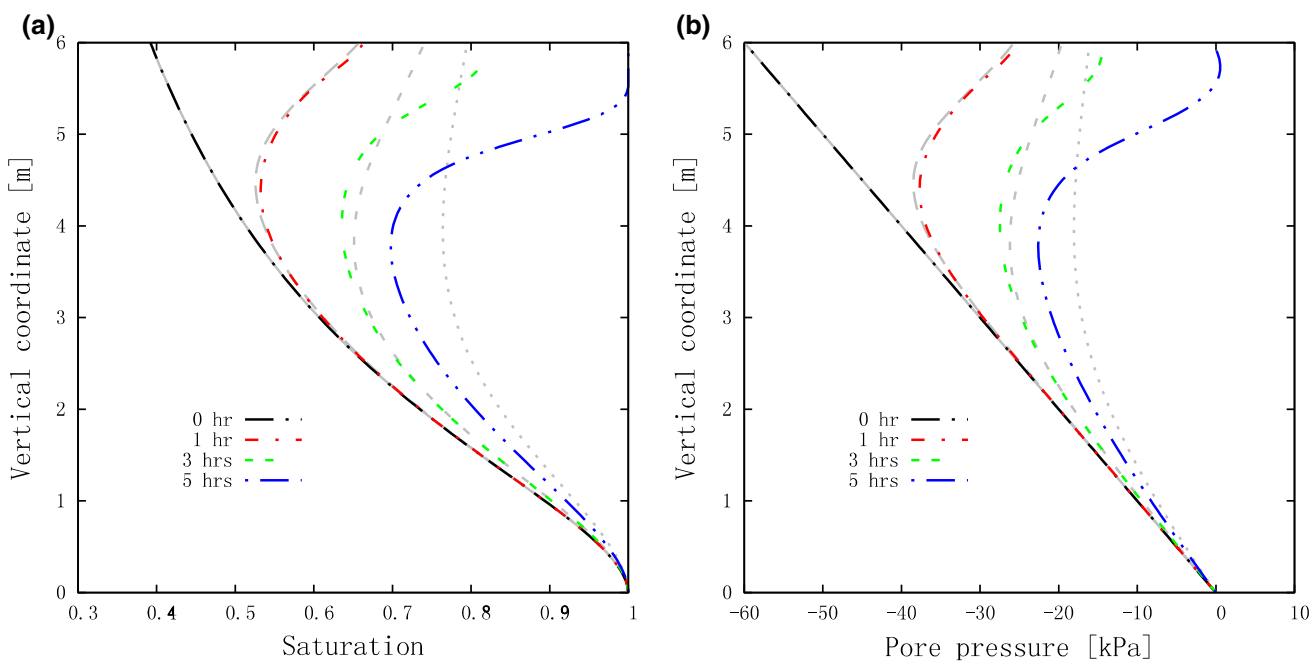


Fig. 13 Profiles of liquid saturation and pore pressure in case 3. **a** Saturation; **b** pore pressure

been totally saturated, whereas the regions below are still unsaturated. Indeed, consistent with the experiment observation of Wang [45] (as shown in Fig. 1), a relatively impermeable layer below the top surface was generated due to fines clogging which prevents further water infiltration [17, 46]. Correspondingly, in this case, the pore pressures in the upper saturated regions are positive, whereas those of the lower regions remain negative at larger times (as shown in Fig. 13b).

5.4 Slope stability analysis

The profiles of saturation and pore pressure corresponding to the three cases simulated in Sect. 5.3 have been presented in Figs. 9 and 13. The safety factor profiles of these cases can be readily to be calculated by Eq. (25) and are presented in Fig. 14. If only the fines detachment is considered (Fig. 14a), along with the rainfall infiltration, the slope surface was coarsened gradually due to the loss of fines [12, 46]. The increase in porosity (surface coarsening) facilitates the rainfall infiltration and makes the upper region maintain relatively higher matric suctions compared to the case without fines migration (grey curves), which may lead to larger safety factors. In other words, if the fine particles are detached and transported downwards without evident deposition (hence permeability impairment), the slope could possibly become more stable during the rainfall infiltration, as shown in this case.

On the other hand, once evident fines deposition process takes place which leads to significant permeability impairment, the deposition of in situ fluidized fines below the slope surface may create a “filter cake formation” (relatively impermeable layer) which leads to the generation of positive excess pore pressure. The enhanced infiltration by erosion at the upper region may further accelerate the failure process above the impervious layer during the saturation phase [4]. As shown in Fig. 14b, the excess pore pressure generated above the dense deposition region decreases the safety factor significantly. After nearly 5-h rainfall, an initial slip surface is located at about 0.25 m below the slope surface. The slip location is generally consistent with the flume tests of Wang et al. [46] and the in situ tests of Chen [3] performed on the same type of soils and with the same slope angle, which declared that the failure surface is located at the depth of about 5–20 cm from the top surface (also shown in Fig. 1).

According to our numerical results, the safety analysis of internal erosion-prone soil slopes at least should take the following effects into account: (1) the advancement of wetting front decreases the matrix suction hence the shear strength of unsaturated soils; (2) the internal erosion leads to surface coarsening in the soil slopes which will promote the water infiltration process; (3) the deposition of in situ fluidized fines below the slope surface will create a relatively impermeable region which may lead to the generation of positive excess pore pressure above the water table. What’s more, though not considered in this paper, the fines

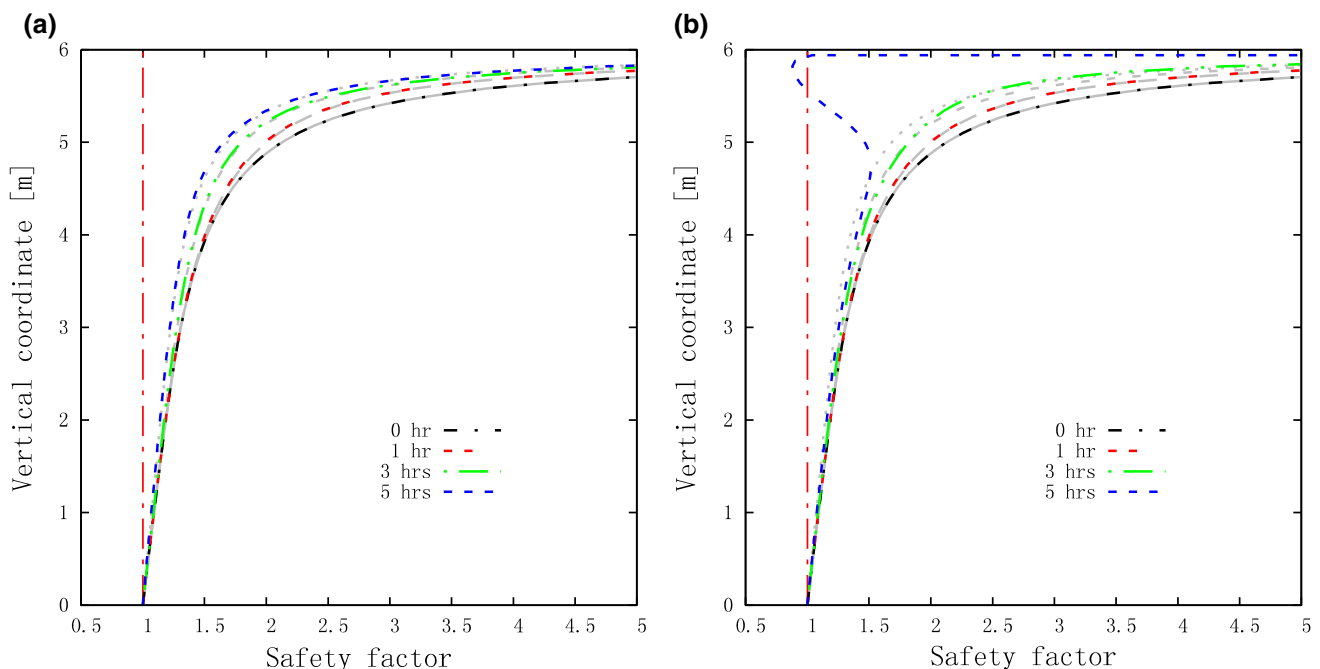


Fig. 14 Safety factor profiles of slopes in case 2 and case 3 (with grey curves corresponding to case 1). **a** Case 2 with erosion; **b** case 3 with erosion and deposition

migration will also alter the mechanical properties of soils more or less [2, 21, 35], which further influences the slope stability.

6 Conclusions

In this paper, the soils susceptible to internal erosion are treated as three-phase multi-species porous media based on mixture theory. Mass conservation equations of liquid phase and fluidized fine particles, together with the empirical rate equations for fines erosion and deposition processes, have been used as governing equations to simulate the rainfall infiltration processes in unsaturated soil columns by the FEM method. It is shown that the erosion and deposition processes influence the infiltration process in a different way. The pure erosion generally increases the soil porosity and facilitates the rainfall infiltration; the deposition process may lead to pore throat blocking and subsequent pore filling, which forms a relatively impermeable layer inside the soil column and prevents the water infiltration through it. Further, an infinite slope model is adopted to analyse the slope stability based on the pore pressure profiles. It is concluded that the erosion process without evident deposition generally promotes the dissipation of pore pressure and therefore may increase the slope stability; however, the fluidized fines may also concentrate below the slope surface to create a relatively impermeable layer, which leads to the generation of positive excess pore pressure and initiates the slope failure. Obviously, the safety of these kinds of slopes cannot be predicted by traditional methods. Therefore, it is advocated that more attention should be paid to the soil slopes which are susceptible to internal erosion.

Acknowledgements Financial support from the NSFC (Nos. 41702331, 41771021, 41472293), Hundred Young Talents Program of IMHE (SDSQB-2016-01), NSFC-ICIMOD (Grant No. 41661144041), “Light of the West” of CAS (Y7R2070070), Youth fund of IMHE (Y7K2050050), the Key Research & Development Program and the Scientific Support Program of the Science & Technology Department of Sichuan Province (Grant No. 2017SZ0041; Grant No. 2016SZ0067) is acknowledged. Also a special acknowledgement should be expressed to Prof. CHEN xiao-qing for his helpful discussions.

References

- Bonelli S (ed) (2012) Erosion of geomaterials. Wiley, Hoboken
- Chang D, Zhang L, Cheuk J (2014) Mechanical consequences of internal soil erosion. HKIE Trans Hong Kong Inst Eng 21(4):198–208. doi:10.1080/1023697X.2014.970746
- Chen XQ (2006) Initiation mechanism of landslide translation to debris flow. Ph.D. Dissertation of Southwest Jiaotong University (in Chinese)
- Chinkulkijniwat A, Yubonchit S, Horpibulsuk S, Jothityangkoon C, Jeebtaku C, Arulrajah A (2016) Hydrological responses and stability analysis of shallow slopes with cohesionless soil subjected to continuous rainfall. Can Geotech J. doi:10.1139/cgj-2016-0143
- Civan F (2015) Reservoir formation damage, 3rd edn. Elsevier, Amsterdam
- Civan F (2016) Modified formulations of particle deposition and removal kinetics in saturated porous media. Transp Porous Media 111(2):381–410. doi:10.1007/s11242-015-0600-z
- Cividini A, Gioda G (2004) Finite-element approach to the erosion and transport of fine particles in granular soils. Int J Geomech 4(3):191–198. doi:10.1061/(ASCE)1532-3641(2004)4:3(191)
- Cividini A, Bonomi S, Vignati GC, Gioda G (2009) Seepage-induced erosion in granular soil and consequent settlements. Int J Geomech 9:187–194
- Collins BD, Znidarcic D (2004) Stability analyses of rainfall induced landslides. J Geotech Geoenviron Eng 130(4):362. doi:10.1061/(ASCE)1090-0241(2004)130:4(362)
- Coussy O (2004) Poromechanics. Wiley, Hoboken, p 312
- Crosta G, di Prisco C (1999) On slope instability induced by seepage erosion. Can Geotech J 36(6):1056–1073. doi:10.1139/99-062
- Cui P, Guo C, Zhou J, Hao M, Xu F (2014) The mechanisms behind shallow failures in slopes comprised of landslide deposits. Eng Geol 180:34–44. doi:10.1016/j.enggeo.2014.04.009
- Fujisawa K, Murakami A, Nishimura S-I (2010) Simultaneous modeling of internal erosion and deformation of soil structures. In: He Q, Shen S-L (eds) Geoenvironmental engineering and geotechnics, vol 50. American Society of Civil Engineers (ASCE), Hannover, pp 71–78. doi:10.1061/41105(378)11
- Galindo-Torres SA, Scheuermann A, Mühlhaus HB, Williams DJ (2015) A micro-mechanical approach for the study of contact erosion. Acta Geotech 10(3):357–368. doi:10.1007/s11440-013-0282-z
- Gardner WR (1958) Some steady state solutions of the unsaturated moisture flow equation with application to evaporation from a water table. Soil Sci 85(4):228–232
- Gruesbeck C, Collins RE (1982) Entrainment and deposition of fine particles in porous media. Soc Petrol Eng J 22:847–856. doi:10.2118/8430-PA
- Guo CX (2015) Research on the fine particle migration in wide grading and poorly consolidated soil. Ph.D. Dissertation of University of Chinese Academy of Sciences (in Chinese)
- Harrison C (2014) On the mechanics of seepage induced cohesionless soil slope instability as applied to foreshore engineering. In: 22nd Vancouver geotechnical society symposium program. <http://v-g-s.squarespace.com/s/Paper-7-Harrison.pdf>
- Iverson RM (2000) Landslide triggering by rain infiltration. Water Resour Res 36(7):1897. doi:10.1029/2000WR900090
- Jian B, Lu X, Wang S, Chen X, Cui P (2005) The movement of fine grains and its effects on the landslide and debris flow caused by raining. Chin J Undergr Space Eng 1(7):1014–1017
- Ke L, Takahashi A (2014) Experimental investigations on suffusion characteristics and its mechanical consequences on saturated cohesionless soil. Soils Found 54(4):713–730. doi:10.1016/j.sandf.2014.06.024
- Khilar KC, Fogler HS (1983) Water sensitivity of sandstones. Soc Petrol Eng J 23(1):55–64. doi:10.2118/10103-PA
- Khilar KC, Fogler HS (1998) Migration of fines in porous media. Kluwer Academic Publishers, Dordrecht
- Lei X, Wong H, Fabbri A, Limam A, Cheng YM (2014) Computers and Geotechnics A thermo-chemo-electro-mechanical framework of unsaturated expansive clays. Comput Geotech 62:175–192. doi:10.1016/j.compgeo.2014.07.004

25. Liu X, Civan F (1993) Characterization and prediction of formation damage in two-phase flow systems. In: SPE production operations symposium. Society of Petroleum Engineers. doi:[10.2118/25429-MS](https://doi.org/10.2118/25429-MS)
26. Loret B, Simões FMF (2005) A framework for deformation, generalized diffusion, mass transfer and growth in multi-species multi-phase biological tissues. *Eur J Mech A Solids* 24(5):757–781
27. Lu N, Godt J (2008) Infinite slope stability under steady unsaturated seepage conditions. *Water Resour Res* 44(11):1–13. doi:[10.1029/2008WR006976](https://doi.org/10.1029/2008WR006976)
28. Lymberopoulos DP, Payatakes AE (1992) Derivation of topological, geometrical, and correlational properties of porous media from pore-chart analysis of serial section data. *J Colloid Interface Sci* 150(1):61–81
29. Marot D, Benamar A (2012) Suffusion, transport and filtration of fine particles in granular soil. In: Bonelli S (ed) *Erosion of geomaterials*. Chapter 2. Wiley, London, pp 39–75
30. Mercier F, Bonelli S, Golay F, Anselmet F, Philippe P, Borghi R (2015) Numerical modelling of concentrated leak erosion during Hole Erosion Tests. *Acta Geotechnica* 10(3):319–332. doi:[10.1007/s11440-014-0349-5](https://doi.org/10.1007/s11440-014-0349-5)
31. Moffat R, Fannin RJ (2011) A hydromechanical relation governing internal stability of cohesionless soil. *Can Geotech J* 48(3):413–424. doi:[10.1139/T10-070](https://doi.org/10.1139/T10-070)
32. Mühlhaus H, Gross L, Scheuermann A (2015) Sand erosion as an internal boundary value problem. *Acta Geotech* 10(3):333–342. doi:[10.1007/s11440-014-0322-3](https://doi.org/10.1007/s11440-014-0322-3)
33. Rahardjo H, Ong TH, Rezaur RB, Leong EC (2007) Factors controlling instability of homogeneous soil slopes under rainfall. *J Geotech Geoenviron Eng* 133(12):1532–1543. doi:[10.1061/\(ASCE\)1090-0241\(2007\)133:12\(1532\)](https://doi.org/10.1061/(ASCE)1090-0241(2007)133:12(1532))
34. Rahmati H, Jafarpour M, Azadbakht S, Nouri A, Vaziri H, Chan D, Xiao Y (2013) Review of sand production prediction models. *J Pet Eng* 2013:1–16. doi:[10.1155/2013/864981](https://doi.org/10.1155/2013/864981)
35. Sato M, Kuwano R (2016) Effects of internal erosion on mechanical properties evaluated by triaxial compression tests. *Jpn Geotech Soc Spec Publ* 2(29):1056–1059. doi:[10.3208/jgssp.JPN-127](https://doi.org/10.3208/jgssp.JPN-127)
36. Sbai MA, Azaroual M (2011) Numerical modeling of formation damage by two-phase particulate transport processes during CO₂ injection in deep heterogeneous porous media. *Adv Water Resour* 34(1):62–82. doi:[10.1016/j.advwatres.2010.09.009](https://doi.org/10.1016/j.advwatres.2010.09.009)
37. Schaufler A, Becker C, Steeb H (2013) Infiltration processes in cohesionless soils. *ZAMM J Appl Math Mech* 93(2–3):138–146. doi:[10.1002/zamm.201200047](https://doi.org/10.1002/zamm.201200047)
38. Scheuermann A, Mühlhaus HB (2015) Infiltration instabilities in granular materials: theory and experiments. *Acta Geotech* 10(3):289. doi:[10.1007/s11440-015-0382-z](https://doi.org/10.1007/s11440-015-0382-z)
39. Tao H, Tao J (2017) Quantitative analysis of piping erosion micro-mechanisms with coupled CFD and DEM method. *Acta Geotech*. doi:[10.1007/s11440-016-0516-y](https://doi.org/10.1007/s11440-016-0516-y)
40. Tsai TL, Chen HF (2009) Effects of degree of saturation on shallow landslides triggered by rainfall. *Environ Earth Sci* 59(6):1285–1295. doi:[10.1007/s12665-009-0116-3](https://doi.org/10.1007/s12665-009-0116-3)
41. Tsaparas I, Rahardjo H, Toll DG, Leong EC (2002) Controlling parameters for rainfall-induced landslides. *Comput Geotech* 29(1):1–27. doi:[10.1016/S0266-352X\(01\)00019-2](https://doi.org/10.1016/S0266-352X(01)00019-2)
42. Uzuoka R, Ichiyama T, Mori T, Kazama M (2012) Hydro-mechanical analysis of internal erosion with mass exchange between solid and water. In: *Proceedings of 6th international conference on scour and erosion*, Paris, pp 655–662
43. Van Genuchten MT (1980) A closed-form equation for predicting the hydraulic conductivity of unsaturated soil. *Soil Sci Soc Am J* 44(5):892–898
44. Vincens E, Witt KJ, Homberg U (2014) Approaches to determine the constriction size distribution for understanding filtration phenomena in granular materials. *Acta Geotech* 10(3):291–303. doi:[10.1007/s11440-014-0308-1](https://doi.org/10.1007/s11440-014-0308-1)
45. Wang ZB (2011) Study on soil pores clogging by particles transport and the slope failure mode of in triggering area of debris flow. Ph.D. Dissertation of Institute of Rock & Soil Mechanics Chinese Academy of Sciences (in Chinese)
46. Wang ZB, Li K, Wang R, Hu MJ (2016) Impact of fine particle content on mode and scale of slope instability of debris flow. *Adv Sci Technol Water Resour* 36(2):35–41 (in Chinese)
47. Zhang L, Zhang LL (2014) Influence of particle transport on slope stability under rainfall infiltration. In: Zhang L, Wang Y, Wang G, Dianqing L (eds) *Geotechnical safety and risk IV*. CRC Press, London, pp 323–328
48. Zhang LL, Zhang J, Zhang LM, Tang WH (2011) Stability analysis of rainfall-induced slope failure—a review. *Geotech Eng* 164(164):299–316. doi:[10.1680/geng.2011.164.5.299](https://doi.org/10.1680/geng.2011.164.5.299)
49. Zhang XS, Wong H, Leo CJ, Bui TA, Wang JX, Sun WH, Huang ZQ (2013) A thermodynamics-based model on the internal erosion of earth structures. *Geotech Geol Eng* 31(2):479–492. doi:[10.1007/s10706-012-9600-8](https://doi.org/10.1007/s10706-012-9600-8)
50. Zhou J, Cui P, Yang X, Su Z, Guo X (2013) Debris flows introduced in landslide deposits under rainfall conditions: the case of Wenjiagou gully. *J Mt Sci*. doi:[10.1007/s11629-013-2492-0](https://doi.org/10.1007/s11629-013-2492-0)
51. Zhuang J, You Y, Chen X, Pei L (2012) Effect of infiltration and anti-scourability of mixed-grain-sized, unconsolidated soil on debris flow initiation. *Bull Soil Water Conserv* 32(4):43–47 (in Chinese)